Exact numerical solutions for dark waves on the discrete nonlinear Schrödinger equation

Bernardo Sánchez-Rey
Departamento de Física Aplicada I, E. U. P., Universidad de Sevilla, Virgen de África 7, 41011 Sevilla, Spain

Magnus Johansson
Department of Physics and Measurement Technology, Linköping University, SE-581 83 Linköping, Sweden
(Received 12 November 2004; published 30 March 2005)

In this paper we study numerically existence and stability of exact dark waves on the (nonintegrable) discrete nonlinear Schrödinger equation for a finite one-dimensional lattice. These are solutions that bifurcate from stationary dark modes with constant background intensity and zero intensity at a site, and whose initial state translates exactly one site each period of the internal oscillations. We show that exact dark waves are characterized by an oscillatory background whose wavelength is closely related with the velocity. Faster dark waves require smaller wavelengths. For slow enough velocity dark waves are linearly stable, but when trying to continue numerically a solution towards higher velocities bifurcations appear, due to rearrangements in the oscillatory tail in order to make possible a decreasing of the wavelength. However, in principle, one might control the stability of an exact dark wave adjusting a phase factor which plays the role of a discreteness parameter. In addition, we also study the regimes of existence and stability for stationary discrete gray modes, which are exact solutions with phase-twisted constant-amplitude background and nonzero minimum intensity. Also such solutions develop envelope oscillations on top of the homogeneous background when continued into moving phase-twisted solutions.

DOI: 10.1103/PhysRevE.71.036627 PACS number(s): 05.45.Yv, 42.65.Wi, 03.75.Lm, 63.20.Ry

I. INTRODUCTION

There is a large current interest in effects arising from competition between nonlinearity and dispersion in spatially periodic systems, which in many cases can be well captured by simple nonlinear lattice models [1]. In particular, much recent experimental activity has been devoted to studies of arrays of nonlinear optical waveguides [2], as well as to studies of Bose-Einstein condensates (BECs) in optical lattices [3]. Under certain conditions (notably strong periodic potentials and, for BECs, a large number of atoms per well), the dynamics can in both cases (Refs. [4,5], respectively) approximately be described by the discrete nonlinear Schrödinger (DNLS) model [Eq. (1) below, see, e.g., Ref. [6] for a review of its properties and applications]. As predicted by the DNLS model, the existence of self-localized discrete solitons has been experimentally confirmed in both contexts (Refs. [7,8], respectively). These are particular examples of a generic class of time-periodic, spatially localized modes in nonlinear lattices, the so-called "intrinsic localized modes" or "discrete breathers" [9].

An important consequence of the discreteness (or spatial periodicity) in these systems is, that self-localization is possible also when the nonlinearity in itself is defocusing (repulsive interactions). This is a result of the band gap structure of the dispersion relation for linear waves, and the anomalous dispersion (or diffraction, in the case of spatial solitons) at the Brillouin zone boundary. In particular, in the DNLS description the attractive and repulsive cases are mathematically equivalent through a "staggering" transformation $(-1)^j$, corresponding to reversing the phases in every second potential well. Thus, in such a situation discrete solitons (breathers) have exponentially decaying staggered tails, and have been observed experimentally in optically induced nonlinear photonic lattices [10], waveguide arrays [11], as well as BECs in periodic potentials [8].

On the other hand, it is well known [12] that without the periodic potential (continuum system), a defocusing nonlinearity generally leads to the existence of dark solitons, consisting of a localized dip in a homogeneous background intensity [like the dark-soliton solution of the defocusing integrable nonlinear Schrödinger (NLS) equation [13]]. Such modes are ubiquitous in nonlinear optics [12], and also observed in BECs with repulsive interatomic interaction (e.g., Ref. [14]). When adding a periodic potential, it is possible to generate stationary discrete dark solitons (breathers) not only in the standard defocusing case, but also for focusing (attractive) nonlinearity where staggered dark solitons may exist, analogously to the staggered bright solitons in the defocusing case. Such staggered discrete (immobile) dark solitons, predicted from the DNLS model [16], have indeed been experimentally observed in waveguide arrays [15,11]. For BECs in optical lattices, dark solitons have not yet been experimentally reported, but theoretically analyzed in Ref. [17].

However, as was found first numerically for the DNLS model in Ref. [16] and later confirmed in Ref. [18], the discreteness may induce oscillatory instabilities for the stationary dark modes. It was found [18], that for infinite chains the strength of these instabilities decay in an exponential-like way approaching the continuum NLS limit, while for finite-size systems stabilization due to boundary effects may occur. Typically, these instabilities lead to a spontaneous motion of the dark mode, together with some radiation [16,18]. It is therefore an interesting question, whether such moving dark solitons (breathers) may exist as exact solutions in the DNLS model, and if so, whether they may be stable in regimes where the stationary dark modes are unstable. Addressing these issues is the main purpose of the present paper.

In integrable models, such as the Ablowitz-Ladik discretization of the NLS equation, traveling dark solitons exist and can be obtained exactly analytically [19]. The evidence that

moving dark breathers may exist as exact solutions in a nonintegrable lattice was given by Feddersen, who showed numerically [20], for the DNLS as well as for the discrete Davydov equations, that traveling dark waves bifurcated from stationary solutions. However, the solutions he found all had a wide envelope and were close to continuum NLS dark solitons. Attempting a continuation towards narrower modes, he found that it always stopped at some point, but he did not analyze this scenario in detail.

On the other hand, much recent attention has been drawn to the study of mobile discrete (bright) breathers in general oscillator chains, and it has been found, numerically [21,22] as well as mathematically [23], that such solutions may exist but typically as nonlocalized solutions with a small-amplitude oscillatory tail. A preliminary calculation of one of the present authors (M.J.) [24] showed, that generally also the tails of numerically exact moving dark DNLS solitons did not have a constant amplitude, but exhibited small-amplitude envelope oscillations (in Ref. [25], such solutions were termed "dark nanopterons"). In addition, it has also been preliminary reported [26], that also stationary gray modes, with nonzero minimum intensity and phase twisted background (cf. gray solitons in continuum NLS models [12]), may exist in the DNLS model. In this paper, we will provide extensive numerical confirmation of these preliminary results. By performing numerical continuations from the stationary dark DNLS soliton, we observe the following main effects of discreteness: (i) An exact moving discrete dark wave generically has envelope oscillations around the constant-amplitude background and (ii) gray solitons with phase-twisted constant-amplitude background exist as stationary solutions trapped by the lattice potential.

It should also be emphasized that, due to the generic nature of the DNLS equation, similar results should be expected also for dark breathers in other types of anharmonic lattice models. Stationary dark breathers have been discussed as well for Klein-Gordon [25,27,28], as for Fermi-Pasta-Ulam (FPU) models [29,30], and the validity of the DNLS approximation for weak coupling and small-amplitude oscillations explicitly confirmed numerically.

The outline of this paper is as follows. In Sec. II we introduce the DNLS model, and recapitulate briefly some properties of its stationary dark modes from [18]. In Sec. III we describe our numerical results for existence and stability of exact traveling dark waves; Sec. III A discusses the continuation versus velocity, and Sec. III B the continuation versus internal frequency, which essentially plays the role of discreteness parameter. Section IV discusses properties of gray solitons with a phase gradient, which may be either stationary or moving. Finally, in Sec. V some concluding remarks are made.

II. STATIONARY DARK MODES

Our starting point is the (attractive) DNLS equation

$$i\dot{\psi}_j + |\psi_j|^2\psi_j + C(\psi_{j+1} + \psi_{j-1} - 2\psi_j) = 0, \tag{1}$$

where $\psi_j(t)$ is the complex amplitude of the oscillator at site j on a lattice, and C is a coupling constant. Without loss of generality, we assume $C>0$. We consider a finite lattice ($j=1,2,\ldots,N$) and adopt, as usual, periodic boundary conditions: $\psi_{j+N}(t)=\psi_j(t)$.

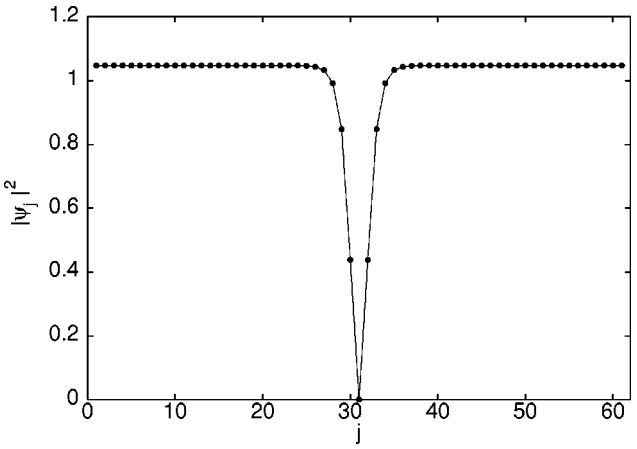

FIG. 1. Stationary dark breather for $\Omega'=\pi/3$, $\omega_0=4$ and $C=1$.

Let us assume that $\psi_j(t)$ is a solution of the DNLS Eq. (1) and define

$$\psi'_j(t) = \psi_j(t)e^{i\omega_0 t}. \tag{2}$$

By direct substitution into (1) it is easy to check that $\psi'_j(t)$ verifies

$$i\dot{\psi}'_j + |\psi'_j|^2\psi'_j + C(\psi'_{j+1} + \psi'_{j-1} - 2\psi'_j) + \omega_0\psi'_j = 0. \tag{3}$$

As a first step we are going to study stationary dark solutions to (3) of the form

$$\psi'_j(t) = \phi_j e^{i\Omega' t}, \tag{4}$$

with time independent ϕ_j and Ω'. These solutions correspond to stationary dark solutions of the DNLS Eq. (1) with frequency $\Omega=\Omega'-\omega_0$. We obtain them numerically (as an example see Fig. 1) by continuation of the code $\ldots+1,-1,+1,-1,0,+1,-1,+1,-1\ldots$ at the anticontinuous limit $C=0$. As it is well known [18], they show a constant background intensity ($|\psi_j|^2\to\Omega+4C; |j|\to\infty$), with zero amplitude at a lattice site.

In particular, we are interested in studying the linear stability of these solutions versus the period $T=2\pi/\Omega'$. Figure 2 shows the moduli of the Floquet eigenvalues for the choice $\omega_0=4$. For low enough values of the period (high enough frequencies, equivalent to anticontinuum limit) the solutions are stable, but increasing T above a critical value $T\simeq 0.48$ we observe oscillatory instabilities. These oscillatory instabilities are size dependent and their computation for increasing system sizes suggests that they decay to zero for large enough T for any finite chain, but only asymptotically for $T\to\infty$ (continuum limit) in the infinite chain. This result is equivalent to the one observed in Ref. [18] for increasing coupling [with the used parameter values, Fig. 2 appears as a rescaling of Fig. 2 in Ref. [18], with $T\leftrightarrow 2\pi C$ and Moduli of Floquet eigenvalues $\leftrightarrow e^{2\pi\mathrm{Re}(\lambda)}$].

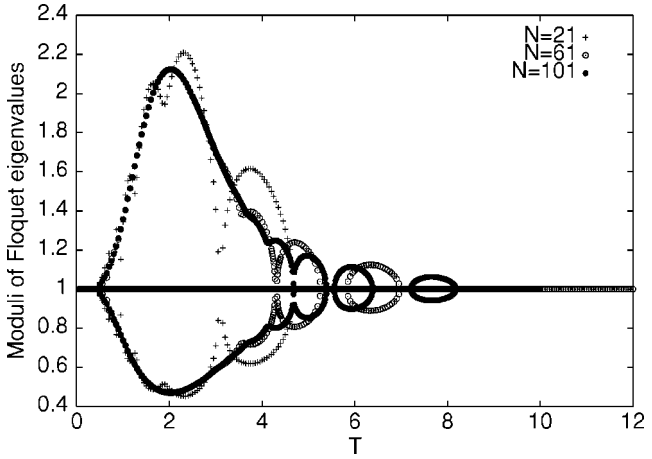

FIG. 2. Oscillatory instabilities of the stationary dark breathers vs the period for different lattice sizes and parameter values $C=1$, $\omega_0=4$.

We remark that, for direct physical applications, the form (3) is generally the most relevant form of the DNLS equation, with ω_0 being the frequency of an uncoupled oscillator in the small-amplitude limit, and $\Omega'=2\pi/T$ a physical oscillation frequency. Thus, the frequency Ω of a solution to (1) normally does not in itself describe a physical oscillation frequency but rather a frequency shift relative to ω_0, and therefore Ω does not need to be sign definite. Evidently, the sign of a frequency also depends on the sign-convention used in (2) and (4).

III. EXACT DARK WAVES

Traveling dark waves were found to appear, together with some radiation, from unstable stationary dark breathers in numerical simulations [16,18,25,27]. Typically these moving dark breathers continuously emit radiation and decay (its minimum intensity increases), especially if the dark mode is narrow. However, analogously to the search for moving 'bright' discrete breathers [21,22], one can search for traveling dark breathers which after m internal oscillations, each of period T, return to a state identical to its initial state but translated k sites. In other words, we can look for solutions to (3) that fulfill

$$\psi_j'(mT) = \psi_{j-k}'(0)e^{i\alpha'}, \tag{5}$$

where α' is some arbitrary phase. The dark solitary wave numerically found in Ref. [20] is a special case of such a solution.

The reason for working with Eq. (3) instead of Eq. (1) is that $\psi_j(t)=\psi_j'(t)e^{-i\omega_0 t}$ will be a solution of Eq. (1) fulfilling the condition $\psi_j(mT)=\psi_{j-k}(0)e^{i\alpha}$ with a phase

$$\alpha = \alpha' - \omega_0 mT. \tag{6}$$

Thus, for fixed parameters C, T, m, and k, we are able to investigate the dependence of an exact mobile solution of the DNLS system on the phase α, just by computing a solution to Eq. (3) of the form (5), and doing the continuation versus ω_0. In other words, for the DNLS model there are no effects of commensurability, in contrast to the case for general oscillator chains [21]. Note that for a stationary dark mode, we must have $\omega_0<(2\pi/T)+4C$ to have a nonzero background intensity, and that continuation in the direction of larger ω_0 (at fixed T and C) towards this limit value is equivalent to approaching the continuum dark-soliton limit, i.e., the "dip" in the envelope becomes wider.

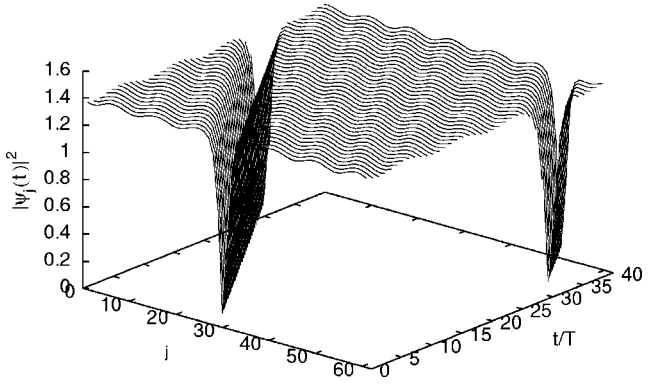

FIG. 3. Time evolution of an exact dark wave. The initial state translates one site each period T of the internal oscillations.

To obtain numerically an exact traveling dark wave, we have imposed in the Newton iteration the condition (5) and, as a guess, we have taken the corresponding stationary solution and applied a sinusoidal perturbation to its imaginary part, which plays a role similar to the velocity in stationary breathers on Klein-Gordon systems. With this method, for $m=1$ and $k=-1$, we have found exact dark solutions moving to the left with a phase $\alpha'=\pi$, which means that

$$\psi_{j-2}'(2T) = \psi_{j-1}'(T)e^{i\pi} = \psi_j'(0). \tag{7}$$

Therefore the envelope velocity of these dark waves is $c=2/2T=1/T$, since the lattice spacing is 1. In Fig. 3 we show the dynamics of an exact dark wave for the case $T=4.5$. Note that Eq. (7) implies that $|\psi_{j-1}'(T)|^2=|\psi_j'(0)|^2$.

In Fig. 4, we show snapshots of dark waves at times when their envelopes are site centered, which is when their dip intensity is minimal. We observe that the minimum intensity of these moving solutions is small but nonzero. In that sense, they are "gray" modes rather than "black" modes. Another important property is that the background intensity is not constant. These waves show a characteristic oscillating tail which seems to be necessary in order to avoid phonon radiation. We can also appreciate that for fixed C and ω_0, the intensity of the background decreases with the velocity. The same behavior is observed for the minimum intensity.

Note that, for a stationary constant-amplitude traveling background wave of the form (4), with $\phi_j=\phi^{(0)}e^{iQj}$, to be compatible with the condition (7), its amplitude must fulfill

$$|\phi^{(0)}|^2 = \frac{Q+(2n+1)\pi}{T} + 2C[1-\cos(Q)] - \omega_0 \tag{8}$$

for some integer n. For large T, the family of solutions in Fig. 4 approaches the stationary dark mode, corresponding to a constant-amplitude background with $n=0$ and $Q=\pi$. When continuing these solutions towards smaller T, the observed

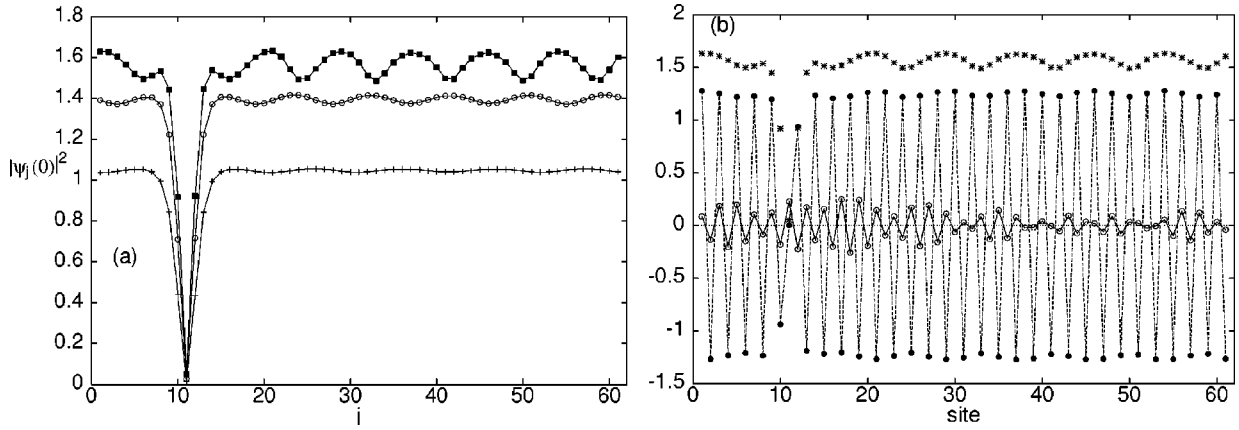

FIG. 4. (a) Snapshots of exact moving dark breathers corresponding to $T=4$, $T=4.5$, and $T=6$ from top to bottom. Note how the intensity of the background decreases when T increases. Other parameters values: $C=1$, $\omega_0=4$. (b) Re$[\psi_n(0)]$ (full circles), Im$[\psi_n(0)]$ (open circles), and $|\psi_n(0)|^2$ (stars) for an exact moving solution with $T=4$.

oscillations develop against a background which still, as illustrated in Fig. 4(b), approximately can be described by (8) with $n=0$ and $Q=\pi$. (In the smooth continuation, the average phase twist is fixed by using periodic boundary conditions in a finite-size system.) Thus, these dark modes move through the interaction with the tail envelope oscillations, and not through an average tail phase gradient e^{iQj}, $Q \neq 0, \pi$. However, solutions with a phase gradient also exist, and we will return to this point in Sec. IV.

One can study the linear stability of these solutions linearizing the map $\epsilon_j(0) \rightarrow \epsilon_{j-1}(T)$ around the exact solution ψ_j'. The linearized equations for ϵ_j are

$$i\dot{\epsilon}_j + 2|\psi_j'|^2(t)\epsilon_j + \psi_j'^2(t)\epsilon_j^* + C(\epsilon_{j+1} + \epsilon_{j-1} - 2\epsilon_j) + \omega_0\epsilon_j = 0. \tag{9}$$

This linearized map defines an extended Floquet matrix with properties analogous to the ordinary Floquet matrix for stationary solutions (cf. Ref. [21]).

A. Continuation versus T

As in the case of stationary dark breathers in finite-size systems, the mobile solutions are stable for high enough values of T (slow enough velocities) if ω_0 is not too small. (In this subsection, we put $\omega_0=4C$, so that $T\rightarrow\infty$ becomes a continuum limit.) If we perform a numerical continuation of this family of stable solutions towards lower values of T (higher velocities) we find bifurcations as Fig. 5 shows. These bifurcations are due to harmonic instabilities (a pair of eigenvalues collides at +1 and leaves the unit circle along the real axis). After emerging the instability the Newton method stops to converge and the continuation path is interrupted. However, we can jump into another family of solutions able to move faster increasing the continuation step. In Fig. 6 we compare a solution just at the bifurcation point $T_1=8.456$ (pluses) whose continuation stops at 8.385 with a solution found increasing the continuation step up to 8.3 (circles). What happens if we continue the latter solution towards the bifurcation point? We observe a fast growth and rearrangements in the oscillatory structure of the tails (see full circles for $T=8.450$ in Fig. 6) until the continuation finally stops at 8.468. The signature of these huge changes in the oscillating tail is an avoided collision at +1 between two conjugated Floquet eigenvalues and the appearance of oscillatory instabilities, as Figs. 7(a) and 7(b) show, respectively.

The following harmonic bifurcations we found in Fig. 5 occur at $T_2\simeq 8.023$, $T_3\simeq 6.872$, $T_4\simeq 6.234$, $T_5\simeq 6.029$, $T_6\simeq 5.034$, and $T_7\simeq 4.604$. For $T<4.1$ more bifurcations appear at $T_8\simeq 4.091$, $T_9\simeq 4.025$, $T_{10}\simeq 3.907$, and $T_{11}\simeq 3.780$ but most of them are not visible because the continuation path is interrupted immediately after a pair of eigenvalues collide at +1. The structure of all these bifurcations is similar to the one described earlier. Figure 8 shows the exact mobile solution at the bifurcation point $T_5=6.029$ (circles), which can be continued until $T=5.797$, and the family of solutions obtained increasing the continuation step up to $T=5.6$ (squares). A three-dimensional plot in Fig. 9 shows the continuation path of this new solution towards the bifurcation point T_5. An avoided collision at +1 occurs at 5.6704 [see Fig. 10(a)]. After the avoided collision the order of the oscillating tail is destroyed. A projection of Fig. 9 on to the $(j,|\psi_j|^2)$ plane (see Fig. 11) shows that this is due to the

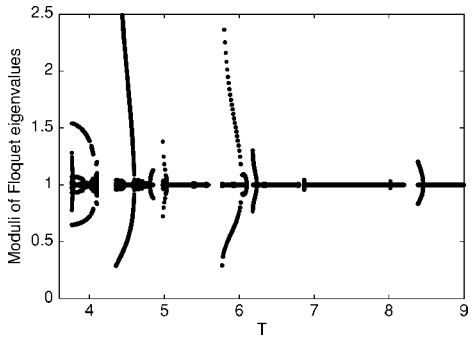

FIG. 5. Instabilities found along a numerical continuation towards lower values of T. Shortly after the harmonic bifurcations the continuation path stops. At this point we have to jump into another family of solutions increasing the continuation step. For $T<7$ we begin to observe oscillatory instabilities which become stronger. Other parameter values: $C=1$, $\omega_0=4$, $N=61$.

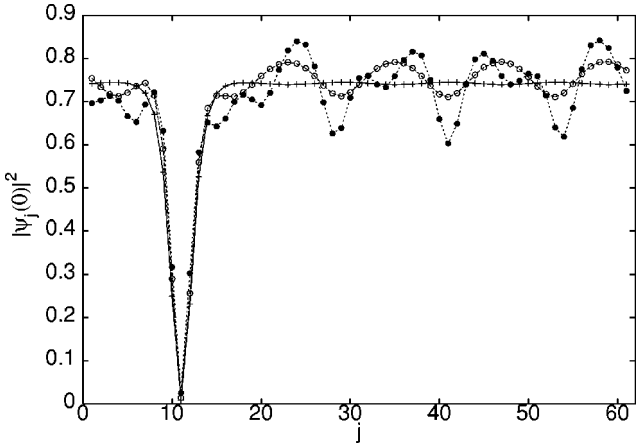

FIG. 6. Exact mobile dark breathers just at the first bifurcation $T_1=8.456$ (pluses) and for $T=8.3$ (circles) after jumping over the bifurcation. The full circles correspond to the continuation of this last solution towards the bifurcation point. Other parameter values: $C=1$, $\omega_0=4$.

activation of an extended mode with wave number close to π. The phenomenon resembles a lot resonances due to higher harmonics observed in Klein-Gordon lattices, e.g., resonances between standing-wave phonons observed in Ref. [25], and the breather-phonon resonance described in Ref.

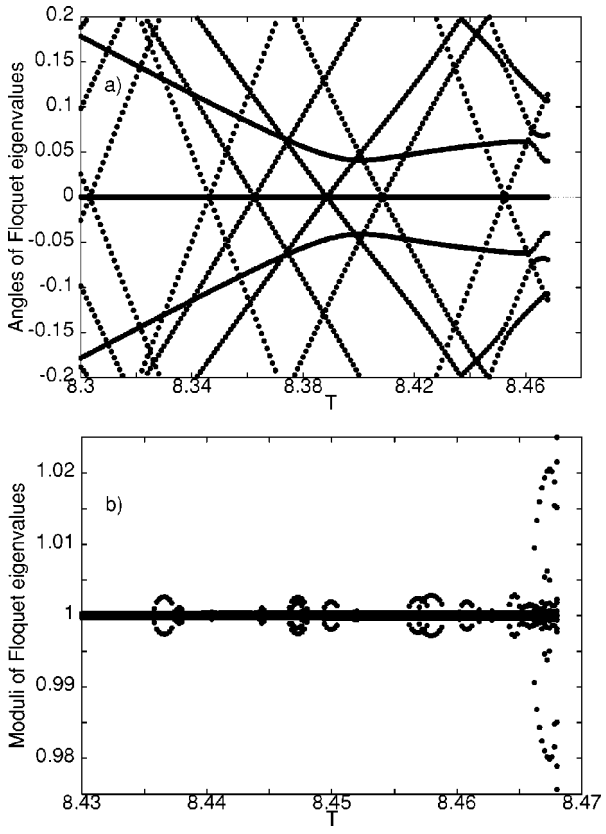

FIG. 7. (a) When we reverse the continuation path after jumping over a bifurcation, an avoided collision between a pair of conjugated Floquet eigenvalues gives raise to huge changes in the oscillatory tail of the solutions. (b) These rearrangements enclose oscillatory instabilities.

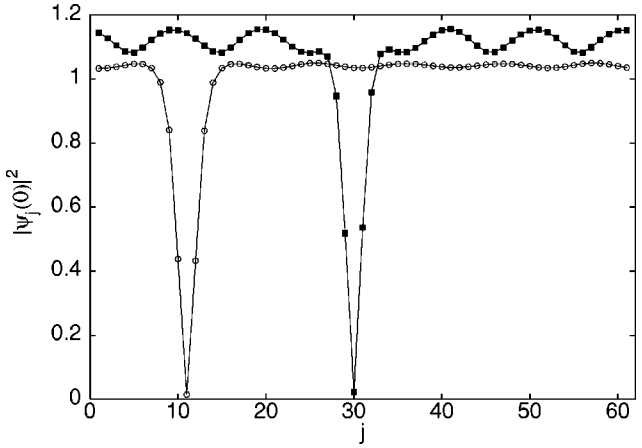

FIG. 8. Exact mobile dark breathers just at the bifurcation $T_5=6.029$ (circles) and for $T=5.6$ (squares) after jumping over the bifurcation. Other parameter values: $C=1$, $\omega_0=4$.

[31] along a breather-phonobreather transition. In Fig. 10(b) we also show the oscillatory instabilities associated with this process.

Small bubbles of oscillatory instabilities are present in the system for $T<7$. They are not visible in Fig. 5 due to the scale on the Y axis. The size of these bubbles increases as T decreases, and in fact we can appreciate them clearly in Fig. 5 for $T<5$.

All the earlier descriptions show that the nature of the oscillating background changes along the continuation path towards smaller T. Clearly, as the velocity increases the number of oscillations increases and, therefore, the number of sites per oscillation decreases. For example, in Fig. 6 we have roughly five oscillations for $T=8.3$ with about 12 sites per oscillation. In Fig. 8 we can appreciate six oscillations with ten sites per oscillation for $T=5.6$. For $T=4.5$ (see Fig. 4) the number of oscillations increases up to seven with approximately nine sites per oscillation. We again can observe seven oscillations for $T=4$ but now with eight sites per oscillation (see Fig. 4 anew). We conclude that the harmonic bifurcations along the continuation towards smaller T are associated with a qualitative change of tail nature, corresponding either to an increase of the number of oscillations, a decrease of the number of sites per oscillation, or both.

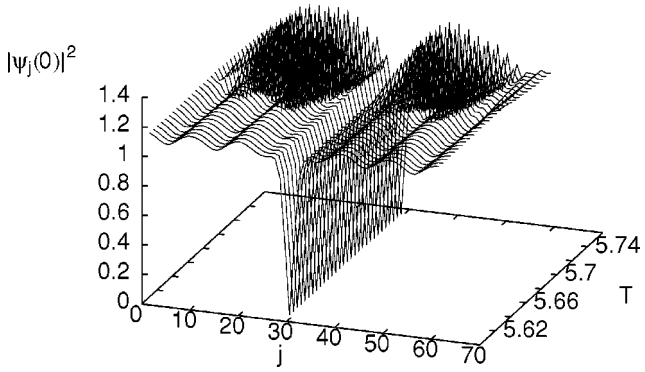

FIG. 9. Inversion of the continuation path after jumping over the fifth bifurcation. When we approach the bifurcation point the smooth oscillating tails are destroyed.

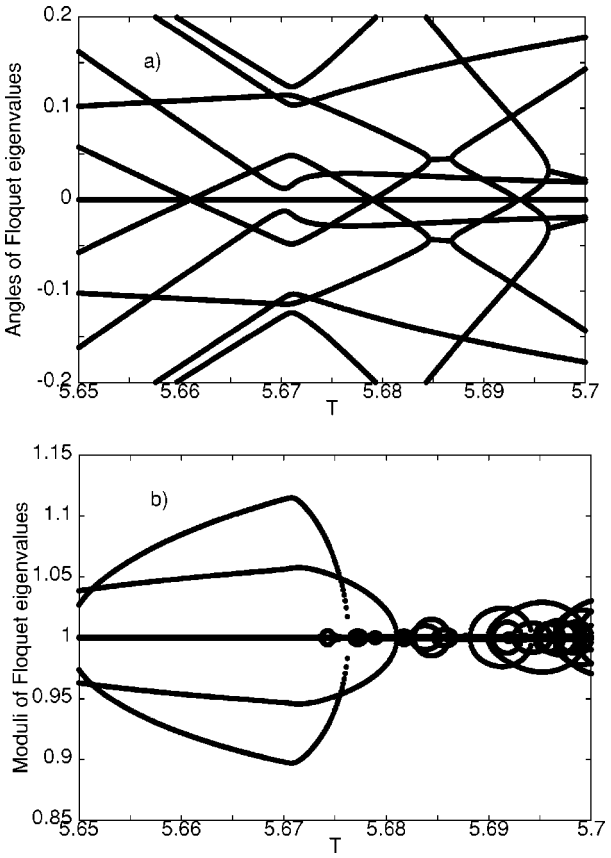

FIG. 10. (a) An avoided collision between a pair of conjugated Floquet eigenvalues points out the excitation of the extended mode shown in Fig. 11. (b) This excitation gives raise to numerous oscillatory instabilities.

We can obtain an analytical estimate for the dependence of the oscillating tail wave number on the velocity, by considering small-amplitude tail oscillations in the linearized equations. With the ansatz for the tail

$$\psi_j'(t) = [\phi^{(0)} + u_0 e^{i(qj+\omega t)} + v_0 e^{-i(qj+\omega t)}] e^{i(\pi j + \Omega' t)}, \quad (10)$$

with $\Omega' = 2\pi/T$ and $\phi^{(0)} = \sqrt{\Omega' - \omega_0 + 4C}$, condition (7) is fulfilled if $\omega T - q = 2\pi n$, n integer. Moreover, inserting the ansatz into (3) and linearizing yields the dispersion relation for small-amplitude oscillations around the stationary solution (cf., e.g., Ref. [32]), $\omega^2 = 8C \sin^2(q/2)[2C \sin^2(q/2) + (\phi^{(0)})^2]$. Combining these two conditions thus determines the possible wave numbers q for small-amplitude tail oscillations at given T, C, ω_0, as

$$q + 2\pi n \pm 4CT \left| \sin \frac{q}{2} \right| \sqrt{\sin^2 \frac{q}{2} + \frac{2\pi - \omega_0 T}{2CT}} + 2 = 0. \quad (11)$$

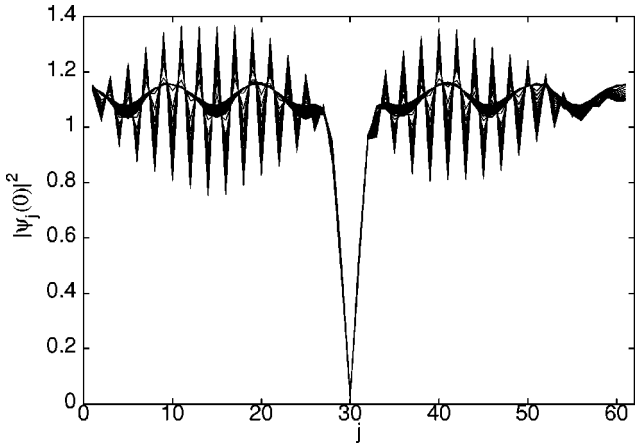

FIG. 11. Projection of Fig. 9 on to the $(j, |\psi_j|^2)$ plane. Notice the excitation of an extended mode with wave number close to π.

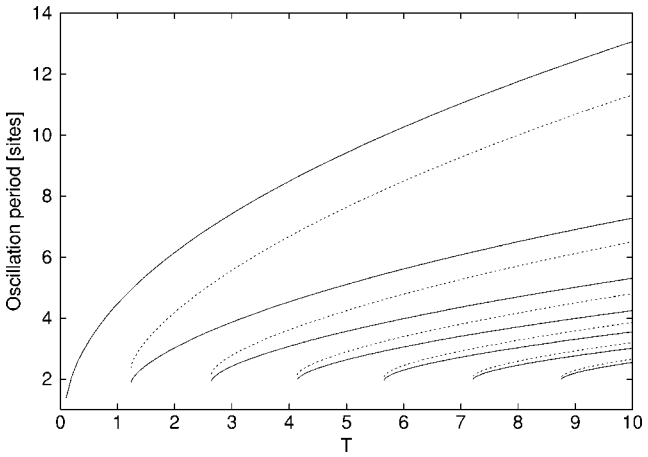

FIG. 12. Spatial oscillation period $2\pi/q$ vs T for small-amplitude tail oscillations of the form (10) fulfilling (7), as obtained from (11). Solid (dashed) lines correspond to a positive (negative) sign in (11), with, from top to bottom, n ranging from -1 to -7 (1 to 6). As in previous figures, $C=1$ and $\omega_0=4$.

The variation of the spatial oscillation period $2\pi/q$ with T for fixed ω_0, C, corresponding to the relevant solutions of (11), is illustrated in Fig. 12. As can be seen, the curve corresponding to a positive sign and $n=-1$ in (11) agrees qualitatively well with the numerical results reported earlier. Note that this solution corresponds to opposite signs of q and ω, and thus a wave traveling to the right, i.e., in the opposite direction to the dark breather itself. Thus, the traveling dark breather emits backward radiation behind at the same time as it absorbs radiation in front, which makes possible its existence as an exact solution.

B. Continuation versus ω_0

For fixed period (fixed velocity) we can also continue a given solution versus the phase parameter ω_0. We find that the background and the stability of the dark waves are very sensitive to this parameter ω_0. When ω_0 decreases, the dark mode narrows and becomes more discrete, and the background intensity and the oscillation amplitudes increase very quickly. As an example, a mobile dark breather for $T=12$ and $\omega_0=4$ (circles in Fig. 13) can be continued until $\omega_0=3.64$. For that value, we can see in Fig. 13 (full circles) that the oscillations are very large. If we increase ω_0, the dark mode widens and becomes more continuumlike, and we observe the opposite effect. For $\omega_0=4.25$ (pluses) the background intensity has already been reduced to its half, and the back-

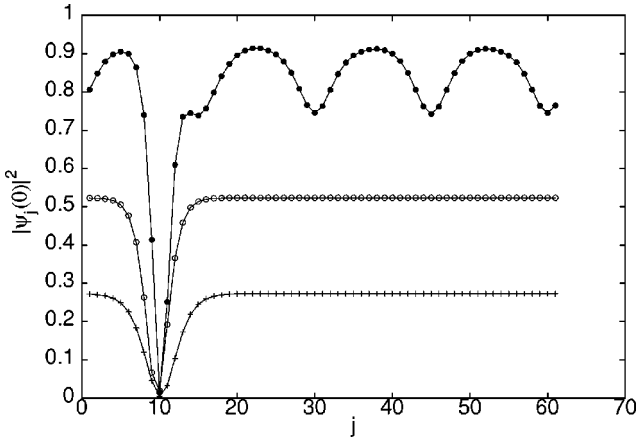

FIG. 13. Exact dark waves for $T=12$ and three different values of ω_0: 4.0 (circles), 3.64 (full circles), and 4.25 (pluses). C=1.

ground oscillations are invisible on the scale of the figure, but still present (they are of order 10^{-6}). This continuation path ends, for the considered system with $N=61$, at $\omega_0=4.516$ (close to the limit value $\omega_0=2\pi/T+4C$ for the stationary mode in the infinite system) with a background intensity around 0.007.

This result is very interesting for various reasons. On the one hand, varying ω_0 one can find stable mobile solutions with huge oscillating tails if the velocity is slow enough. An example is the solution shown in Fig. 13 with full circles.

On the other hand, for a given unstable mobile solution one can adjust the phase ω_0 in order to stabilize it. In Fig. 14 we show how we can avoid the harmonic instability at $T=8.4<T_1$ decreasing ω_0. Another alternative would be to jump into another stable family of dark mobile solutions increasing the continuation step from $\omega_0=4.013$ (where the continuation path stops) to $\omega_0=4.02$.

For higher velocities the scenario becomes more complex due to the appearance of more and stronger instabilities. But again we can find windows of stability managing ω_0 as Fig. 15 shows for the case $T=5$.

The bifurcations observed in the continuations versus ω_0 at fixed T are essentially the same types of bifurcations as

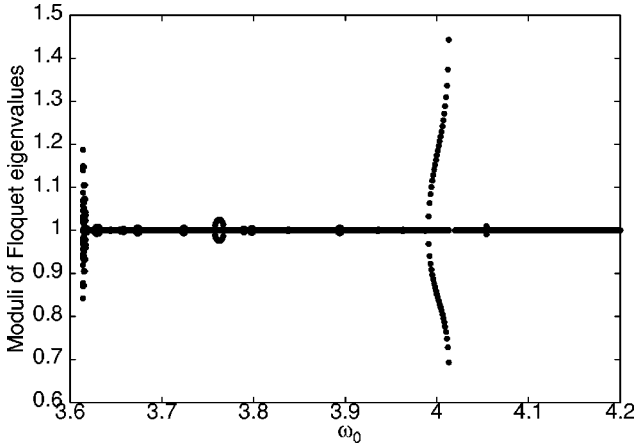

FIG. 14. Instabilities vs the phase ω_0 for a fixed value of the period $T=8.4$.

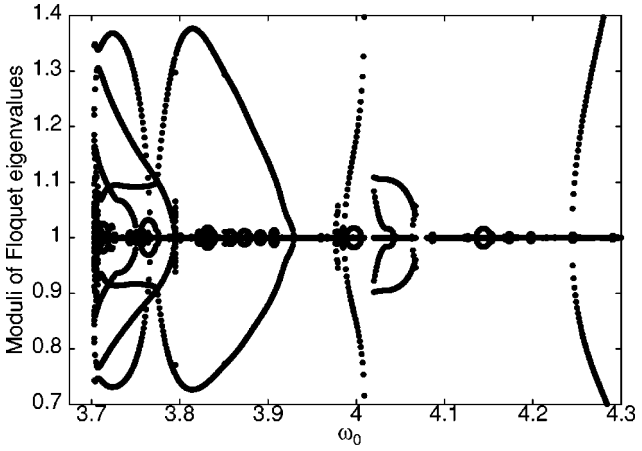

FIG. 15. Instabilities vs the phase ω_0 for a fixed value of the period $T=5$.

those discussed in Sec. III A in the continuation versus T at fixed ω_0. Generally, since we have two-parametric families of solutions, each bifurcation should define a bifurcation curve in the (ω_0,T) plane [cf., e.g., a similar scenario for second-harmonic resonances of standing waves in Klein-Gordon chains, illustrated in Ref. [25], Fig. 16(a)]. Performing the continuations at fixed T and fixed ω_0, respectively, we will generally hit these curves from different directions. Note also that expression (11) for the linear resonances depends not only on T but also on ω_0, since the background amplitude depends on ω_0. Thus, the linear spatial oscillation period changes also when varying ω_0 at fixed T, so that a similar set of resonances should be expected (and is also numerically observed) also in this continuation. (Another way of expressing this is, that the bifurcation curves in the (ω_0,T) plane generally are not horizontal or vertical lines.)

IV. STATIONARY AND MOVING GRAY SOLITONS WITH PHASE GRADIENT

From a "quasicontinuum" NLS approximation of the DNLS Eq. (3), taking into account the discrete dispersion for the background wave $\phi^{(0)}e^{i(Qj+\Omega' t)}$ but neglecting other effects of discreteness, one finds [16] that the envelope velocity c and the minimum intensity $|\psi_{min}|^2$ for wide, continuum-like discrete dark solitons should be related by

$$c = 2C\sin(Q) \pm |\psi_{min}|. \tag{12}$$

Thus, the minimum intensity determines the envelope velocity relative to the group velocity of the background wave. It also determines the total phase shift across such a solution (relative to the background wave) as $\delta=2\arccos|\psi_{min}/\phi^{(0)}|$. In particular, the quasicontinuum NLS approximation predicts the existence of a stationary ($c=0$) gray soliton with $|\psi_{min}|=2C\sin(Q)$. The condition $|\psi_{min}|<|\phi^{(0)}|$ would thus limit the existence of such solutions to $|2C\sin(Q)/\phi^{(0)}|<1$.

However, as was discussed in Ref. [16], the quasicontinuum NLS approximation does in general not accurately describe wide small-amplitude [ψ_{min} close to $\phi^{(0)}$] gray solitons in the discrete system, since it does not take into ac-

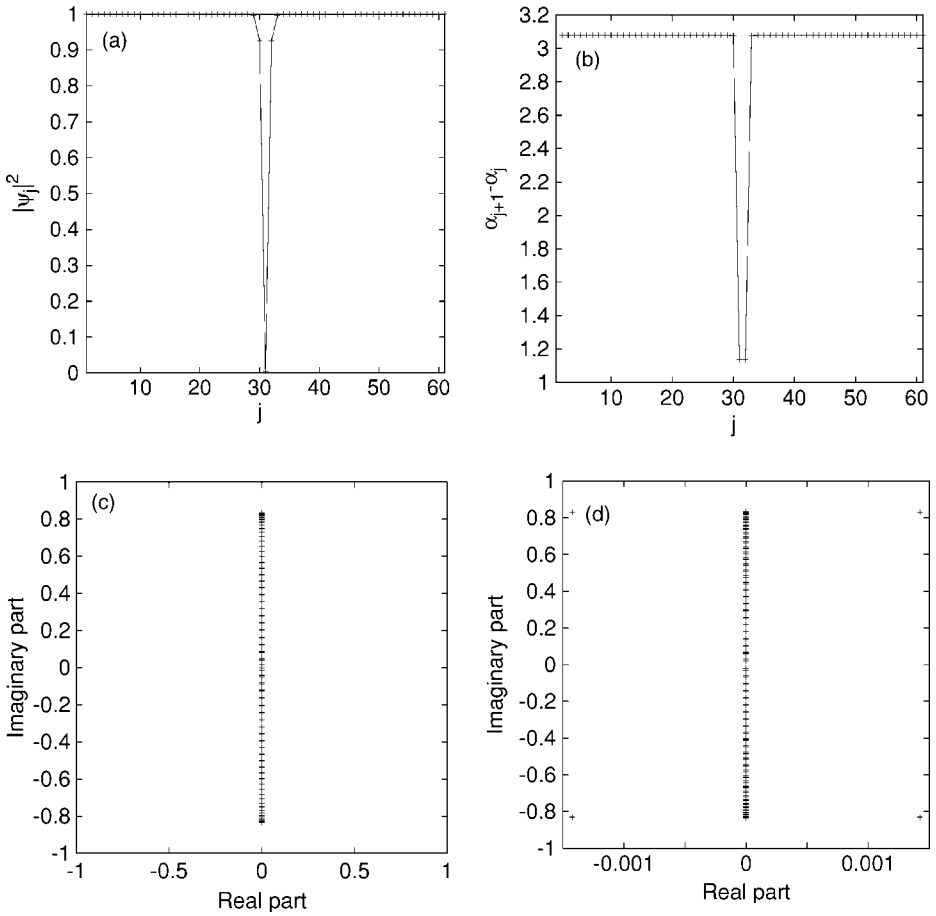

FIG. 16. Stationary discrete gray breather in DNLS, corresponding to a background wave with $Q=0.98\pi$. (a) shows, for $C=0.075$, intensity $|\psi_j|^2$ (minimum intensity is $|\psi_{31}|^2\approx 0.0052$); (b) shows nearest-neighbor phase shifts $\alpha_{j+1}-\alpha_j$ (with notation $\psi_j=|\psi_j|e^{i\alpha_j}$) (note that the total phase shift across the central site $\alpha_{32}-\alpha_{30}$ is *not* π as it would be for a black breather). Lower figures with stability eigenvalues show that the solution is close to the threshold of Krein instability: $C=0.075$ is stable (c) while $C=0.076$ is unstable (d).

count effects of higher-order dispersion. Instead, by taking into account also third and fourth-order dispersion in the continuum approximation and performing a multiscale expansion, it is possible to derive a Korteweg-de Vries (KdV) equation for the soliton amplitude in the limit of small amplitude (see also Ref. [33]). The envelope of the corresponding family of soliton solutions, parametrized by the small parameter μ, can be written as [16]:

$$|\psi_j(t)| = \phi^{(0)} - \frac{12\mu^2 G_2}{G_1}\,\mathrm{sech}^2[\mu(n-(V_g+c_0+W)t)], \tag{13}$$

where $V_g=2C\sin(Q)$, $c_0^2=-2[\phi^{(0)}]^2C\cos(Q)$, $G_1=4\phi^{(0)}C\cos(Q)[-3+V_gc_0/4C^2\cos^2(Q)]$, $G_2=C^2\cos^2(Q)[1+(\phi^{(0)})^2/6C\cos(Q)]-V_gc_0/3$, and $W=-2\mu^2G_2/c_0$. (In Ref. [16] only the case $V_g=0$ was considered, leading to a vanishing third-order dispersion. However, the third-order dispersion present when $V_g\neq 0$ only leads to a renormalization of the coefficients in the KdV equation; see also Ref. [34].) Thus, the condition for a stationary small-amplitude gray soliton becomes $V_g+c_0+W=0$. The limit of vanishing soliton amplitude $\mu^2G_2\to 0$ then gives the limit for existence of a stationary gray solution as $V_g=-c_0$, i.e., it may exist when

$$\left|\frac{2C\sin^2(Q)}{[\phi^{(0)}]^2\cos(Q)}\right| < 1, \tag{14}$$

which notably agrees with the expression obtained from the quasicontinuum NLS limit only when $|\tan(Q)|=1$. (Note that, as was discussed in Ref. [16], the family (13) of solutions also exists for $G_2/G_1<0$, leading to "antidark" pulses.)

To search numerically for stationary gray solutions as exact solutions to the DNLS Eq. (3), we impose the boundary conditions $\phi_{N+1}=e^{iQ}\phi_N$, $\phi_0=e^{-iQ}\phi_1$ and perform a continuation versus Q, using the dark (black) solutions with $Q=\pi$ and $\phi^{(0)}=1$ previously obtained [18] for $C>0$ as trial solutions in the Newton scheme, with an additional phase torsion e^{iQj} imposed on the background. (Our method is analogous to that used in Ref. [35] for Klein-Gordon lattices.) To keep the background intensity to unity, we vary the frequency Ω as $\Omega=1+2C[\cos(Q)-1]$. An example with $Q=0.98\pi$ is shown in Fig. 16. This solution can be continued towards larger C, and generally becomes smoother and "grayer" (i.e., $|\psi_{min}|$ increases) as C is increased for fixed Q. The scenario with oscillatory (Krein) instabilities is similar to the scenario for the black solitons [18] as long as Q is close to π. However, some qualitative differences in the continuation scenario are observed:

(i) For each Q, $\pi/2<Q<\pi$, there is a maximum value of C for existence of a stationary gray mode. To numerical accuracy, this maximum value is given by $C_{max}(Q)=|\cos(Q)|/2\sin^2(Q)$ as predicted by (14), and corresponds to the point where $|\psi_{min}|=\phi^{(0)}$, and the smooth continuumlike gray soliton bifurcates with the plane wave with wave number Q. Note that C_{max} is a monotonously increasing function of Q in the interval $[\pi/2,\pi[$, with $C_{max}(\pi/2)=0$ and $C_{max}(\pi)\to+\infty$.

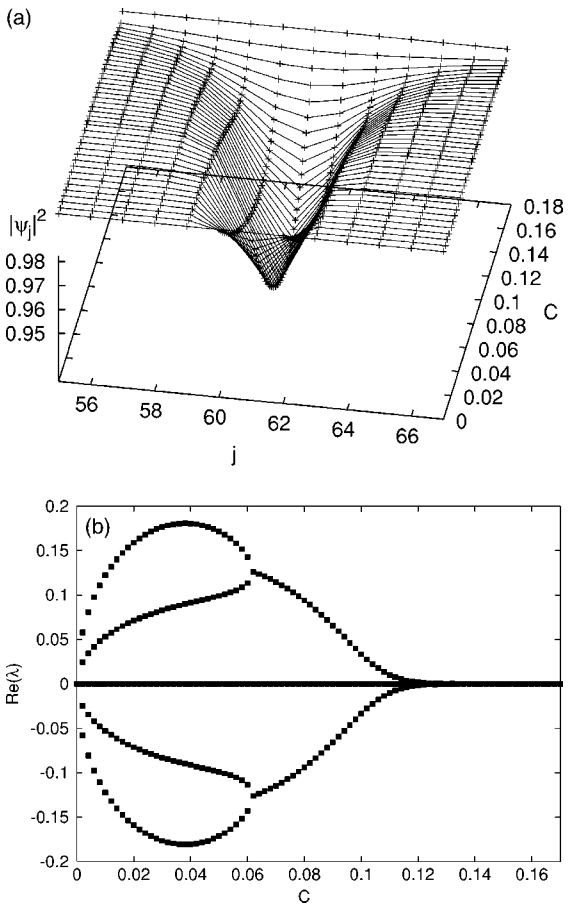

FIG. 17. (a) Continuation of stationary discrete gray soliton from continuous limit $C=C_{max}$ [from (14)] to anticontinuous limit $C=0$ at fixed $Q=0.6\pi$. The smallest minimum intensity $|\psi_{min}|^2 \simeq 0.9398$ is obtained for $C\simeq 0.09$. Only the central part of a larger chain is shown. (b) shows the real part of the stability eigenvalues during the continuation. The unstable eigenvalues are complex for $C\gtrsim 0.06$ and real for $C\lesssim 0.06$.

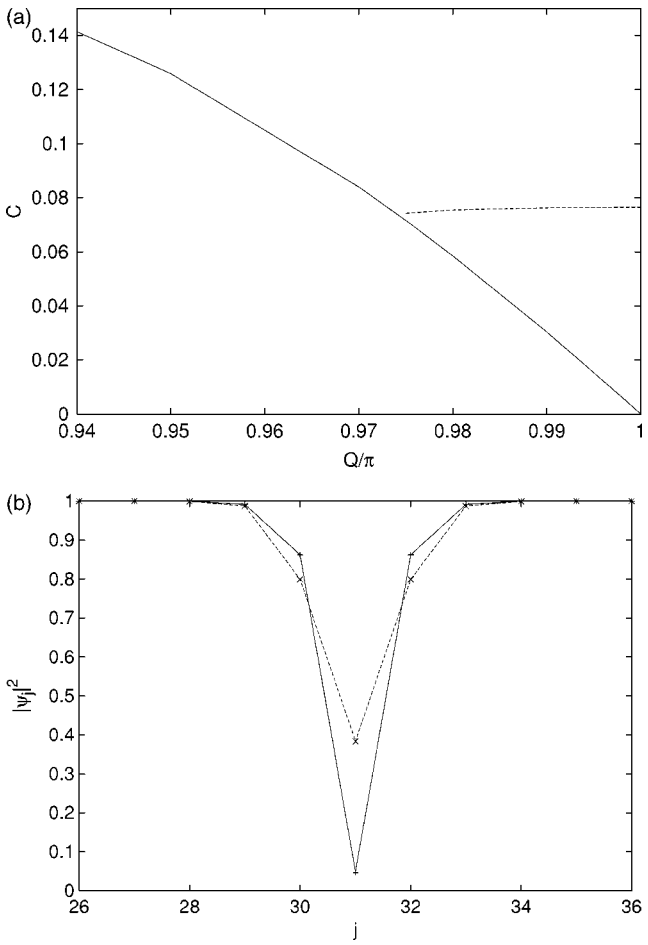

FIG. 18. (a) Solid line: Location of the bifurcation interrupting a monotonic continuation at fixed Q of a continuumlike gray soliton towards the anticontinuous limit $C=0$. Dashed line: Location of the Krein collision causing oscillatory instability. A stable stationary discrete gray soliton exists only in the area between the lines (lower right part of the figure). (b) Patterns for the central parts of two simultaneously existing solutions at $Q=0.95\pi$, $C=0.13$. (+): Solution continued from continuous limit; (×): solution continued from anticontinuous limit.

(ii) Attempting a continuation towards the anticontinuous limit $C=0$ at fixed Q, there are two possible qualitatively different scenarios depending on Q. For $\pi/2<Q\lesssim 0.92\pi$ the continuation is monotonic, and ends at the constant-amplitude phase-twisted solution $(\ldots, e^{-2iQ}, e^{-iQ}, +1, e^{iQ}, -1, e^{-iQ}, +1, e^{iQ}, e^{2iQ}, \ldots)$, at $C=0$, where the "−1" denotes the central site. The total phase twist with respect to the background wave at the anticontinuous limit is thus $\delta=2(2Q-\pi)$. The scenario is illustrated in Fig. 17 for $Q=0.6\pi$. Thus, for each Q there is an "optimal" value of C where the stationary gray soliton contrast is largest. Note also that the instability scenario is different than for $Q=\pi$: the unstable complex eigenvalues behave similarly close to the continuum limit, but when decreasing C they do not return to the imaginary axis but collide with each other on the real axis, so that close to the anticontinuous limit there are two unstable real eigenvalues. Thus, strictly speaking, the gray solitons are always unstable for infinite systems for these Q.

For $0.92\pi\lesssim Q\lesssim\pi$, a monotonic continuation of the continuumlike gray soliton to the anticontinuous limit $C=0$ at fixed Q is not possible due to a bifurcation, associated with a collision of eigenvalues at $\lambda=0$. The location of this bifurcation line in the Q-C plane is illustrated in Fig. 18(a). Similarly, the continuation of the anticontinuous solution discussed earlier to larger C is now interrupted by another bifurcation close to $C=0.14$ (depends only weakly on Q). Thus, there is a region in the Q-C plane where these two solutions exist simultaneously, but have different properties [see Fig. 18(b)]. The solution continued from the anticontinuous limit is always unstable, while the solution continued from the continuous limit is stable only in the area in the lower right corner in Fig. 18(a), above which the oscillatory instability sets in. Thus, stable stationary discrete gray solitons only exist (for the infinite chain) for $0\leqslant C\lesssim 0.076$ and $0.975\lesssim Q/\pi\leqslant 1$.

In a similar way as described in Sec. III, it is possible to find also exact moving gray discrete solitons with an average phase torsion $Q\neq\pi$, by using perturbations of the stationary

gray solitons discussed in this section as trial solutions. In general, we find that these solutions have qualitatively similar properties as those with a background $Q=\pi$ wave, i.e., typically they develop spatial envelope oscillations on top of the homogeneous background when continued away from their continuum limit, with similar bifurcation scenarios as described in Sec. III.

V. CONCLUSIONS

In this paper we have investigated numerically existence and linear stability of exact dark waves on the DNLS equation, for a finite chain with periodic boundary conditions. These waves bifurcate from stationary modes with zero intensity at a site. The initial state of the exact dark waves we have found, translate exactly one site each period T of the internal oscillations. They are linearly stable for slow enough velocities (large T), but when we continue them towards higher velocities oscillatory and harmonic instabilities arise. The first are similar to oscillatory instabilities shown by dark stationary modes from which dark waves bifurcate. The harmonic instabilities are associated with rearrangements in the oscillating background due to the fact that higher velocities require an increase of the number of oscillations in the background.

For fixed velocity, we have also studied the dependence of exact dark waves on the phase factor introduced during the translation, which essentially plays the role of discreteness parameter for the dark modes. The stability and the intensity of the dark waves are very sensitive to this parameter. In principle, one could control the background and the stability of the dark wave if one were able to adjust this phase factor.

We have also investigated stationary gray DNLS solitons, having backgrounds with constant intensity and phase torsion and nonzero minimum intensity, and determined regimes for their existence and stability. Similarly as the previously studied black modes, gray modes also suffer oscillatory instabilities persisting close to the continuum limit. For infinite systems, stable stationary gray solitons were found only in a small parameter regime, at small coupling constant C and background wave number Q close to π.

ACKNOWLEDGMENTS

M.J. would like to thank Yu. S. Kivshar for initiating his interest in the topic, and A. M. Morgante for discussions at an early stage of this project. B.S.-R. acknowledges financial support from Ministerio de Ciencia y Tecnología of Spain under Grant No. BFM2003-03015. M.J. acknowledges support from the Swedish Research Council.

[1] D. K. Campbell, S. Flach, and Yu. S. Kivshar, Phys. Today **57**, 43 (2004).
[2] D. N. Christodulides, F. Lederer, and Y. Silberberg, Nature (London) **424**, 817 (2003).
[3] L. Fallani, L. DeSarlo, J. E. Lye, M. Modugno, R. Saers, C. Fort, and M. Inguscio, Phys. Rev. Lett. **93**, 140406 (2004).
[4] D. N. Christodoulides and R. I. Joseph, Opt. Lett. **13**, 794 (1988).
[5] A. Trombettoni and A. Smerzi, Phys. Rev. Lett. **86**, 2353 (2001); A. Smerzi and A. Trombettoni, Chaos **13**, 766 (2003).
[6] J. C. Eilbeck and M. Johansson, in *Localization and Energy Transfer in Nonlinear Systems*, edited by L. Vázquez, R. S. MacKay, and M. P. Zorzano (World Scientific, Singapore, 2003), p. 44; e-print nlin.PS/0211049.
[7] H. S. Eisenberg, Y. Silberberg, R. Morandotti, A. R. Boyd, and J. S. Aitchison, Phys. Rev. Lett. **81**, 3383 (1998).
[8] B. Eiermann, T. Anker, M. Albiez, M. Taglieber, P. Treutlein, K. P. Marzlin, and M. K. Oberthaler, Phys. Rev. Lett. **92**, 230401 (2004); Th. Anker *et al.*, *ibid.* **94**, 020403 (2005).
[9] S. Flach and C. R. Willis, Phys. Rep. **295**, 181 (1998).
[10] J. W. Fleischer, T. Carmon, M. Segev, N. K. Efremidis, and D. N. Christodoulides, Phys. Rev. Lett. **90**, 023902 (2003); Nature (London) **422**, 147 (2003).
[11] D. Mandelik, R. Morandotti, J. S. Aitchison, and Y. Silberberg, Phys. Rev. Lett. **92**, 093904 (2004).
[12] Yu. S. Kivshar and B. Luther-Davies, Phys. Rep. **298**, 81 (1998).
[13] V. E. Zakharov and A. B. Shabat, Zh. Eksp. Teor. Fiz. **64**, 1627 (1973) [Sov. Phys. JETP **37**, 823 (1973)].
[14] S. Burger, K. Bongs, S. Dettmer, W. Ertmer, K. Sengstock, A. Sanpera, G. V. Shlyapnikov, and M. Lewenstein, Phys. Rev. Lett. **83**, 5198 (1999); J. Denschlag *et al.*, Science **287**, 97 (2000).
[15] R. Morandotti, H. S. Eisenberg, Y. Silberberg, M. Sorel, and J. S. Aitchison, Phys. Rev. Lett. **86**, 3296 (2001).
[16] Yu. S. Kivshar, W. Królikowski, and O. A. Chubykalo, Phys. Rev. E **50**, 5020 (1994).
[17] P. G. Kevrekidis, R. Carretero-Gonzalez, G. Theocharis, D. J. Frantzeskakis, and B. A. Malomed, Phys. Rev. A **68**, 035602 (2003); N. G. Parker, N. P. Proukakis, C. F. Barenghi, and C. S. Adams, J. Phys. B **37**, S175 (2004).
[18] M. Johansson and Yu. S. Kivshar, Phys. Rev. Lett. **82**, 85 (1999).
[19] V. E. Vekslerchik and V. V. Konotop, Inverse Probl. **8**, 889 (1992).
[20] H. Feddersen, in *Nonlinear Coherent Structures in Physics and Biology*, edited by M. Remoissenet and M. Peyrard (Springer, Berlin, 1991), p. 159; Phys. Scr. **47**, 481 (1993).
[21] S. Aubry and T. Cretegny, Physica D **119**, 34 (1998); T. Cretegny, Ph.D. thesis, École normale supérieure de Lyon, France, 1998.
[22] S. Flach and K. Kladko, Physica D **127**, 61 (1999); J. Gómez-Gardeñes, F. Falo, and L. M. Floría, Phys. Lett. A **332**, 213 (2004).
[23] G. Iooss and K. Kirchgässner, Commun. Math. Phys. **211**, 439 (2000); Y. Sire and G. James, C. R. Acad. Sci., Ser. I: Math. **338**, 661 (2004).
[24] M. Johansson, as discussed in Ref. [27], Sec. 4.2.1, and in Ref. [25], footnote 18.
[25] A. M. Morgante, M. Johansson, G. Kopidakis, and S. Aubry,

Physica D **162**, 53 (2002).
[26] M. Johansson (unpublished).
[27] A. M. Morgante, Ph.D. thesis, Ecole Polytechnique, Palaiseau, France, 2001.
[28] A. Alvarez, J. F. R. Archilla, J. Cuevas, and F. R. Romero, New J. Phys. **4**, 72 (2002).
[29] V. Bortolani, A. Franchini, and R. F. Wallis, Phys. Rev. B **56**, 8047 (1997).
[30] B. Sánchez-Rey, G. James, J. Cuevas, and J. F. R. Archilla, Phys. Rev. B **70**, 014301 (2004); A. V. Gorbach (private communication).
[31] A. M. Morgante, M. Johansson, S. Aubry, and G. Kopidakis, J. Phys. A **35**, 4999 (2002).
[32] Yu. S. Kivshar and M. Peyrard, Phys. Rev. A **46**, 3198 (1992).
[33] O. A. Chubykalo, V. V. Konotop, and L. Vázquez, Phys. Rev. B **47**, 7971 (1993).
[34] Yu. S. Kivshar, Phys. Rev. A **42**, 1757 (1990); **43**, 1677 (1991); Yu. S. Kivshar and V. V. Afanasjev, *ibid.* **44**, R1446 (1991).
[35] T. Cretegny and S. Aubry, Phys. Rev. B **55**, R11929 (1997).